International Journal of Science and Research (IJSR)
ISSN (Online): 2319-7064
Index Copernicus Value (2015): 78.96 | Impact Factor (2015): 6.391

Elastic Electron Scattering from Some Proton-Rich Exotic Nuclei

Ahmed N. Abdullah

Department of Physics, College of Science, University of Baghdad, Baghdad, Iraq

Abstract: ***The ground-state properties such as the neutron, proton and matter densities and the associated rms radii of proton-rich ^{8}B and ^{17}Ne halo nuclei are calculated using single-particle radial wave functions of Woods-Saxon (WS) potential. It found that the structure of the halo proton in ^{8}B is a pure $(1p_{1/2})$ and the structure of the two halo protons in ^{17}Ne is mixed configurations with dominant $(2s_{1/2})^2$. Elastic electron scattering form factors of these halo nuclei are also studied by the plane wave Born approximation. Effects of the long tail behavior of the charge density distribution on the charge form factors of ^{8}B and ^{17}Ne are analyzed. It is found that the difference between the charge form factor of ^{8}B and that of stable isotope ^{10}B (or of ^{17}Ne and that of stable isotope ^{20}Ne) is attributed to the influence of the charge density distributions of the last proton in ^{8}B (or of the last two protons in ^{17}Ne).***

PACS number(s): 25.30.Bf, 21.10.Gv.

Keywords: Proton-rich nuclei, Elastic electron scattering, Woods-Saxon potential.

1. Introduction

Nuclear halo is a well-known phenomenon in nuclear physics. Tanihata*et al.* found that the neutron-rich nucleus ^{11}Li had an abnormally large matter root-mean-square radius [1,2]. Further experiments confirmed that there are neutron halo in other neutron-rich nuclei such as ^{6,8}He, ^{11,14}Be, ^{17}B, and ^{19}C [3–5]. Neutron halo manifest themselves as extended neutron density distributions in exotic neutron-rich nuclei. The cause of occurrence of the halo phenomenon lies in both the small separation energy of the last few nucleons and their occupation on the orbits with low angular momentum.

Many experiments [6–9] have been performed to study neutron halo in neutron-rich nuclei and neutron-halo nuclei are well identified in light mass region. Theoretically neutron halos in exotic nuclei ^{6,8}He, ^{11}Li, ^{11,14}Be, ^{17}B, and ^{19}C have also been well reproduced by various theoretical models [10–15]. Although neutron halo have been well investigated in neutron-rich nuclei, studies on proton halo are relatively less. Theoretically, much effort has been made to the search of proton halo in proton drip-line nuclei. Calculations show that there may be proton halo in ^{26,27,28}P [16,17], ^{8}B, ^{17}Ne, and the excited state of ^{6}Li and ^{17}F. Experiments also show some indications of the existence of proton halos in these nuclei [18–21]. However, further experiments are needed to confirm the existence of the proton halo. Thus, the proton halo phenomenon is a very interesting subject of investigation.

Electron-nucleus scattering has proven to be an excellent tool for the study of nuclear structure, especially for the research of electromagnetic properties of nuclei. It has provided much reliable information on charge density distributions of stable nuclei. Thus, we consider that the electron-nucleus scattering is a better way for the precise investigation of the extended charge distribution of the exotic proton-rich nuclei. Unfortunately the electron scattering on exotic nuclei was not possible in the past because of the difficulty of making targets from unstable nuclei. Recently a new collider of electron and unstable nucleus is under construction at RIKEN in Japan [22]. A similar collider at GSI in Germany [23] was also approved by the German government and will be built immediately. So the scattering of electron from unstable nuclei will be available soon. These new facilities will provide a good opportunity to study the charge density distributions of unstable nuclei by elastic electron scattering. Therefore, it is interesting to make an exploratory investigation of elastic electron scattering from proton-rich nuclei.

In the present study, the ground-state properties such as the neutron, proton and matter densities and the associated rms radii of proton-rich ^{8}B and ^{17}Ne halo nuclei are calculated within single-particle radial wave functions of Woods-Saxon (WS) potential. Elastic electron scattering form factors for these nuclei is studied through combining the charge density distribution with the plane wave Born approximation (PWBA). Effects of the long tail behavior presented in the charge density distribution on the form factors of ^{8}B and ^{17}Ne are investigated.

2. Theory

The ground state matter density distribution of exotic (halo) nuclei can be expressed as [24]:

$$\rho_m(r) = \rho^p(r) + \rho^n(r), \tag{1}$$

where $\rho^p(r)$ and $\rho^n(r)$ are the ground state proton and neutron densities of halo nuclei and expressed as:

$$\rho^g(r) = \rho_c^g(r) + \rho_v^g(r) \qquad , g = p, n \tag{2}$$

where $\rho_c^g(r)$ and $\rho_v^g(r)$ are the core and halo (valence) densities and they are calculated through Woods-Saxon (WS) radial wave functions [25] and can be written as:

$$\rho_c^g(r) = \frac{1}{4\pi}\sum_{nlj} X_{nlj,c}^{g} \left|R_{nlj}(r)\right|^2 \tag{3}$$

$$\rho_v^g(r) = \frac{1}{4\pi} X_{nlj,v}^{g} \left|R_{nlj}(r)\right|^2 \tag{4}$$

Where X^{g}_{nlj} represents the number of neutrons or protons, in the sub-shell *nlj*. The $R_{nlj}(r)$ in eqs.(3) and (4) is the solution of the radial of Schrödinger equation [26]:

$$\frac{\hbar^2}{2m}\frac{d^2R_{nlj}(r)}{dr^2}+\left[\varepsilon_{nlj}-V(r)-\frac{\hbar^2}{2m}\frac{l(l+1)}{r^2}\right]R_{nlj}(r)=0 \quad (5)$$

Where ε_{nlj} is the single-particle energy.

For the local potential $V(r)$, the Woods-Saxon shape is used in the compact form [27,28]:

$$V(r)=V_0(r)+V_{so}(r)\vec{\ell}.\vec{s}+V_c(r), \quad (6)$$

where $V_0(r)$ is the spin-independent central potential:

$$V_0(r)=\frac{-V_0}{1+[e^{(r-R_0)/a_0}]} \quad (7)$$

$V_{so}(r)$ is the spin-orbit potential:

$$V_{so}(r)=V_{so}\frac{1}{r}\left[\frac{d}{dr}\frac{1}{1+[e^{(r-R_{ro})/a_{so}}]}\right] \quad (8)$$

and $V_c(r)$ is the Coulomb potential generated by a homogeneous charged sphere of radius R_c [29]:

$$V_c(r)=\frac{Ze^2}{r} \quad \text{for} \quad r\geq R_c \quad (9)$$

$$V_c(r)=\frac{Ze^2}{R_c}\left[\frac{3}{2}-\frac{r^2}{2R_c^2}\right] \quad \text{for} \quad r\leq R_c \quad (10)$$

The radii R_0, R_{so} and R_c are usually expressed as:

$$R_i=r_i A^{1/3} \quad (11)$$

From the proton density $\rho_p(r)$ and the intrinsic charge distribution f_p of one proton, one can obtain the charge distribution of the nucleus with the following folding relation [30]:

$$\rho_{ch}(r)=\int \rho_p(r) f_p(r'-r)dr' \quad (12)$$

The root mean square (rms) radii of the neutron, proton and charge distributions can be obtained from eqs. (2) and (12) as follows [30]:

$$r_g=\left\langle r_g^2\right\rangle^{1/2}=\left[\frac{\int r^2\rho_g(r)dr}{\int \rho_g(r)dr}\right]^{1/2}, g=n,p,ch \quad (13)$$

The elastic electron scattering form factors from considered nuclei are studied by the plane wave Born approximation (PWBA). In the PWBA, the incident and scattered electron waves are represented by plane waves. The elastic electron scattering form factor is simply given by the Fourier-Bessel transform of the ground state charge density distribution (CDD) [31], *i.e.*

$$F(q)=\frac{4\pi}{Z}\int_0^\infty \rho_{ch}(r)\, j_0(qr)\, r^2 dr, \quad (14)$$

where

$$j_0(qr)=\sin(qr)/qr \quad (15)$$

is the zeroth order spherical Bessel function, q is the momentum transfer from the incident electron to the target nucleus and the $\rho_{ch}(r)$ is the CDD of the ground state.

3. Results and Discussion

The nuclear ground state properties of proton-rich ^{8}B (S_{1p}=0.136 MeV , $\tau_{1/2}$=770ms) and ^{17}Ne (S_{2p}=0.933 MeV, $\tau_{1/2}$=109.2ms) [32,33] halo nuclei have been calculated using single-particle radial wave functions of Woods-Saxon (WS) potential. These nuclear properties include the neutron, proton and matter densities and the associated rms radii. Elastic electron scattering form factors for these nuclei is studied through combining the charge density distribution with the plane wave Born approximation (PWBA).

The ^{8}B (J^{π},T=2^{+},1) is one proton halo nucleus composed of the core ^{7}Be (J^{π},T=3/2^{-},1/2) plus one loosely bound proton (J^{π},T=1/2^{-},1/2) surrounding the core whereas the ^{17}Ne (J^{π},T=1/2^{-},3/2) is two-proton Borromean halo nucleus composed of the core ^{15}O (J^{π},T=1/2^{-},1/2) plus two loosely bound protons (J^{π},T=0^{+},1) surrounding the core. The configurations $\{(1s_{1/2})^4, (1p_{3/2})^3\}$ and $\{(1s_{1/2})^4, (1p_{3/2})^8, (1p_{1/2})^3\}$ are assumed for core nuclei ^{7}Be and ^{15}O, respectively. The halo proton in ^{8}B is assumed to be in a pure $1p_{1/2}$. The two halo protons in ^{17}Ne are assumed to be in the model space of HASP which includes the orbitals $1d_{3/2}$, $2s_{1/2}$, $2p_{3/2}$ and $1f_{7/2}$. The occupation numbers of the two halo protons occupying the model space HASP (in ^{17}Ne) are obtained by the computer code NushellX@MSU [34] using the realistic interaction of VPNP [35]. The ground state occupation numbers for the two halo protons in ^{17}Ne are 0.251 for $(1d_{3/2})^2$, 1.57 for $(2s_{1/2})^2$, 0.129 for $(1f_{7/2})^2$ and 0.05 for $(2p_{3/2})^2$. These occupation numbers indicate that the structure of the two halo protons in ^{17}Ne is mixed configurations with dominant $(2s_{1/2})^2$.

Table 1 displays the parameters of Woods-Saxon V_0, V_{so}, r_0, r_{so}, a_0, a_{so} and r_c employed in the present calculations for selected nuclei. The calculated neutron, proton, charge and matter rms radii for ^{8}B and ^{17}Ne nuclei along with the experimental data [36,37] are shown in Tables 2 and 3. It is clear from these tables that the obtained results are in a good agreement with experimental data within quoted error. Besides, the difference between the calculated proton and neutron rms radii for selected halo nuclei is given in Table 2. This difference indicates a definite degree of halo structure of these nuclei. The calculated single-particle energies (ε) for the investigated nuclei along with those obtained by the shell model NushellX@MSU code [34] are tabulated in Table-4. It is clear from this table that the obtained values of the single-particle energies are in excellent agreement with the results of the shell model NushellX@MSUcode.

Table 1: The Woods-Saxon parameters employed in the present calculations for nuclei under study

Nuclei	V_0 (MeV)		V_{so} (MeV)	a_0= a_{so} (fm)		r_0= r_{so} (fm)		r_c (fm)
	Proton	Neutron		Proton	Neutron	Proton	Neutron	
^{8}B	50.750	60.750	6.0	0.650	0.805	1.121	1.394	1.249
^{10}B	49.587	49.587	6.0	0.542	0.542	1.236	1.236	1.306
^{17}Ne	46.552	55.973	6.0	0.717	0.717	1.269	1.269	1.463
^{20}Ne	50.617	50.617	6.0	0.754	0.754	1.479	1.479	1.442

Table 2: The calculated neutron and proton rms radii along with experimental results

Nuclei	$\langle r_n^2 \rangle_{cal}^{1/2}$	$\langle r_n^2 \rangle_{exp}^{1/2}$ [36,37]	$\langle r_p^2 \rangle_{cal}^{1/2}$	$\langle r_p^2 \rangle_{exp}^{1/2}$ [36,37]	$\langle r_p^2 \rangle^{1/2} - \langle r_n^2 \rangle^{1/2}$
^{8}B	2.3	2.31±0.05	2.53	2.53±0.13	0.23
^{17}Ne	2.57	2.69±0.07	3.29	2.79±0.07	0.72

Table 3: The calculated charge and matter rms radii compared with the experimental data.

Nuclei	$\langle r_{ch}^2 \rangle_{cal}^{1/2}$	$\langle r_{ch}^2 \rangle_{exp}^{1/2}$ [36,37]	$\langle r_m^2 \rangle_{cal}^{1/2}$	$\langle r_m^2 \rangle_{exp}^{1/2}$ [36,37]
^{8}B	2.58	-----	2.45	2.45±0.1
^{17}Ne	3.35	2.90±0.07	3.01	2.84±0.23

Table 4: The calculated single-particle energies along with results of the Ref. [34].

Nuclei	nl_j	*proton*		*neutron*	
		ε_{cal} (MeV)	ε (MeV) [34]	ε_{cal} (MeV)	ε (MeV) [34]
^{8}B	$1s_{1/2}$	25.691	25.691	31.111	31.111
	$1p_{3/2}$	14.169	14.169	15.129	15.129
	$1p_{1/2}$	0.9	0.9	----	----
^{17}Ne	$1s_{1/2}$	23.824	23.824	34.533	34.533
	$1p_{3/2}$	11.716	11.716	20.667	20.667
	$1p_{1/2}$	7.861	7.861	17.417	17.417
	$1d_{3/2}$	0.653	0.653	----	----
	$2s_{1/2}$	0.569	0.569	----	----
	$1f_{7/2}$	0.463	0.463	----	----
	$2p_{3/2}$	0.311	0.311	----	----

The calculated matter density distributions and the experimental data (denoted by the shaded area) for ^{8}B [36] and ^{17}Ne [38] halo nuclei are depicted in Figs. 1(a) and 1(b), respectively. The dashed curves correspond to the matter density, while the blue and red curves refer to the calculated neutron and proton densities, respectively. As shown in Fig.1, a good agreement between the calculated results and experimental data was obtained. Moreover, it is evident from this figure that the proton density distributions in these nuclei have a long tail compared with the neutron density distributions, which provides the halo structure of these nuclei.

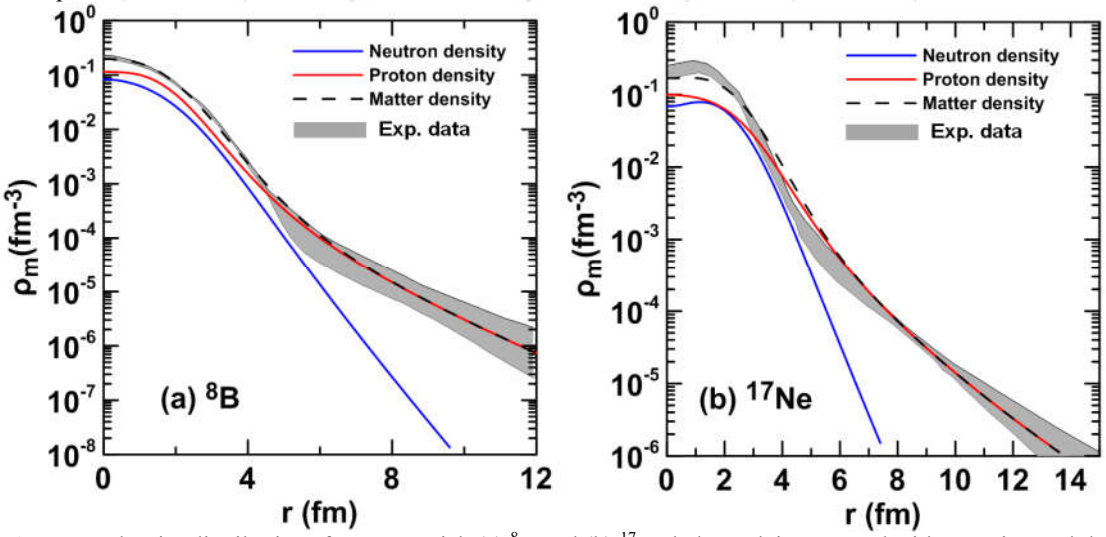

Figure 1: Matter density distributions for proton-rich (a) ^{8}B and (b) ^{17}Ne halo nuclei compared with experimental data (the shaded area)

Figs. 2(a) and 2(b) exhibit the charge density distributions of ^{10,8}B and ^{20,17}Ne, respectively. Therein, the charge density distributions of unstable (^{8}B,^{17}Ne) and stable (^{10}B,^{20}Ne) nuclei are portrayed by the dashed and solid curves, respectively. It is obvious from Fig. 2(a) [Fig. 2(b)] that the charge density distribution of ^{8}B [^{17}Ne] and ^{10}B [^{20}Ne] isotopes are quite different although the number of the protons within these nuclei is the same. The charge density distribution of ^{8}B [^{17}Ne] has a longer tail than that of ^{10}B [^{20}Ne] due to the weak binding of the outer proton [two protons] in ^{8}B [^{17}Ne].

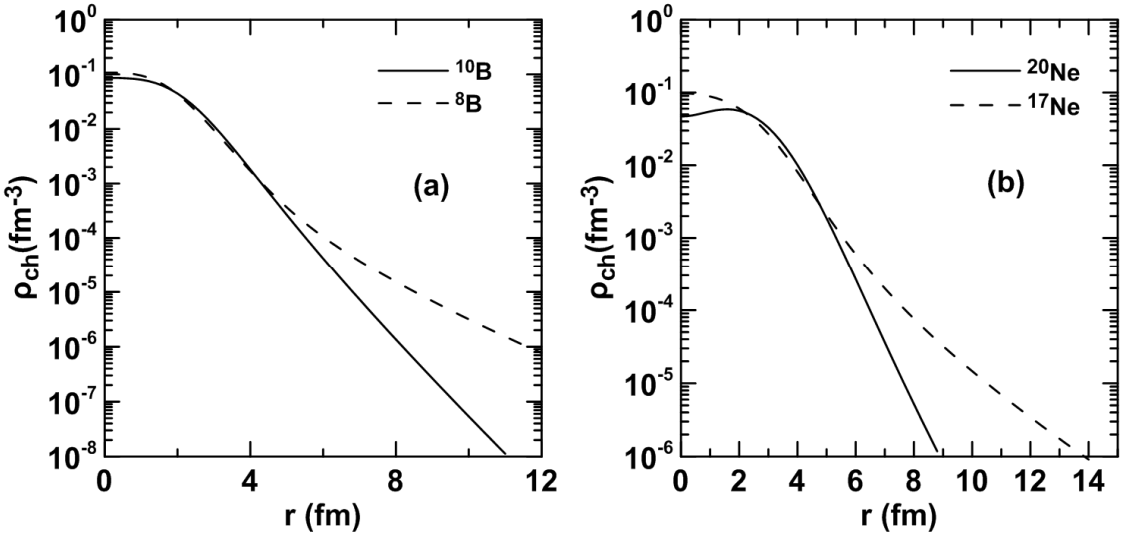

Figure 2: Calculated charge density distributions of proton-rich (a) ^{8}B and (b) ^{17}Ne halo nuclei compared with those of their stable isotopes ^{10}B and ^{20}Ne, respectively

The elastic charge form factors of $^{10,8}B$ and $^{20,17}Ne$ calculated with PWBA are presented in Figs. 3(a) and 3(b), respectively, where the input charge density distributions are those of Figs. 2(a) and 2(b), respectively. The calculated form factors of the unstable (^{8}B, ^{17}Ne) nuclei are displayed by the dashed curves and those of stable (^{10}B, ^{20}Ne) nuclei by solid ones. For comparison the experimental elastic charge form factors of stable ^{10}B [39] and ^{20}Ne [40] are displayed by filled circle symbols.

It is can be seen from these figures that there are significant differences between the calculated form factors of the unstable nuclei (^{8}B, ^{17}Ne) (dashed curves) and stable nuclei (^{10}B, ^{20}Ne) (solid curves). It is clearly noticed in Fig. 3(a), that each of the dashed curve and the solid curve has only one diffraction minimum and one maximum, while those in Fig. 3(b) each has two diffraction minima and two maxima. The location of the minimum of the halo ^{8}B has outward shift as compared with the minimum of a stable ^{10}B. Also, the position of the first and the second minimum of halo ^{17}Ne have an outward shift as compared with the first and the second minimum of stable ^{20}Ne. The significant difference between the charge form factors of the unstable (^{8}B, ^{17}Ne) nuclei and that of stable (^{10}B, ^{20}Ne) nuclei is attributed to the influence of the charge density distributions of the last proton in ^{8}B (or the last two protons in ^{17}Ne).

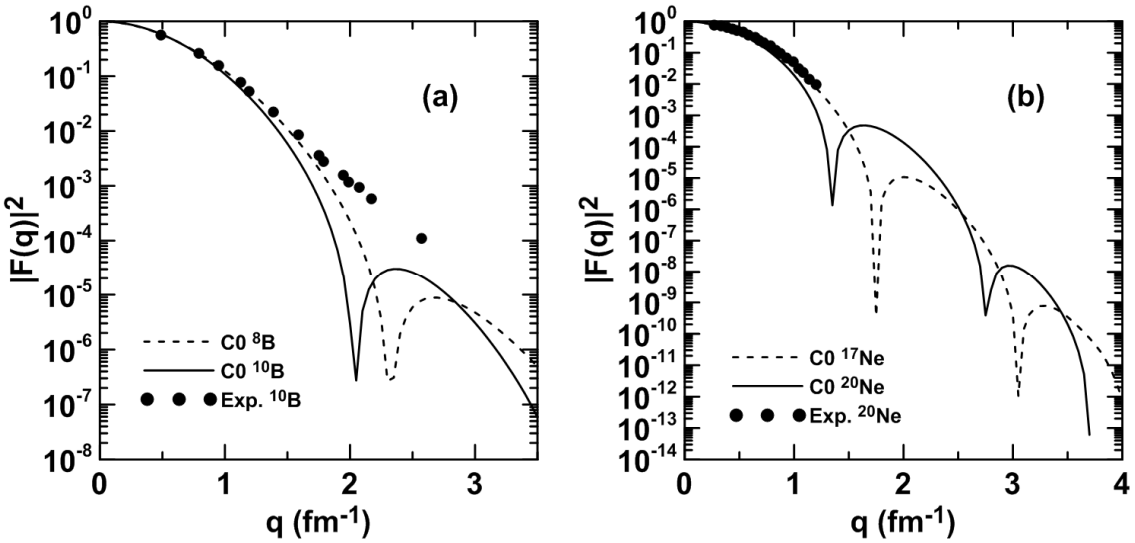

Figure 3: Calculated charge form factors of proton-rich (a) ^{8}B and (b) ^{17}Ne halo nuclei compared with those of their stable isotopes ^{10}B and ^{20}Ne, respectively

4. Summary and Conclusions

The ground-state properties such as the neutron, proton and matter densities and the associated rms radii of proton-rich ^{8}B and ^{17}Ne halo nuclei are calculated using single-particle radial wave functions of Woods-Saxon (WS) potential. Elastic electron scattering form factors of these halo nuclei are also studied by the plane wave Born approximation. Effects of the long tail behavior of the charge density

distribution on the charge form factors of ^{8}B and ^{17}Ne are analyzed. The present study gives the following conclusions:

1) The calculated proton and matter density distributions of ^{8}B and ^{17}Ne halo nuclei exhibit a long tail performance, which is presumed as a distinctive property of halo nuclei.
2) An extra support for the halo structure of these halo nuclei is found due to the noticeable difference between the calculated overall proton and neutron root mean square radii.
3) The analysis of the present study suggests that the structure of the halo proton in ^{8}B is a pure $(1p_{1/2})$ and the structure of the two halo protons in ^{17}Ne is mixed configurations with dominant $(2s_{1/2})^2$.
4) The significant difference between the charge form factor of ^{8}B and that of stable isotope ^{10}B (or of ^{17}Ne and that of stable isotope ^{20}Ne) is attributed to the influence of the charge density distributions of the last proton in ^{8}B (or the last two protons in ^{17}Ne).

References

[1] I. Tanihata*et al*., *Phys. Rev. Lett*. **55**, 2676 (1985).
[2] I. Tanihata*et al*., *Phys. Lett.* B **206**, 592 (1988).
[3] W. Mittig*et al*., *Phys. Rev. Lett.* **59**, 1889 (1987).
[4] T. Kobayashi *et al*., *Phys. Rev. Lett.* **60**, 2599 (1988).
[5] M. G. Saint-Laurent *et al*., *Z. Phys.* A **332**, 457 (1989).
[6] T. Nilsson *et al*., *Nucl. Phys.* A **598**, 418 (1996).
[7] M. Zinser *et al*., *Phys. Rev*. C **70**, 034303 (2004)
[8] N. A. Orr *et al*., *Phys. Rev. Lett*. **69**, 2050 (1992).
[9] R. Anne *et al*., *Phys. Lett.* B **250**,19 (1990).
[10] Z. Ren and G. Xu, *Phys. Lett*. B **252**, 311 (1990).
[11] G. F. Bertsch and H. Esbensen, *Ann. Phys.* (N.Y.) **209**, 327(1991).
[12] M. V. Zhukov *et al*., *Phys. Rep*. **231**, 151 (1993).
[13] P. G. Hansen, A. S. Jensen, and B. Jonson, *Annu. Rev. Nucl. Part. Sci*. **45**, 591 (1995).
[14] J. S. Al-khalili, J. A. Tostevin, and I. J. Thompson, *Phys. Rev.* C **54**, 1843 (1996).
[15] T. Otsuka, N. Fukunishi, and H. Sagawa, Phys. Rev. Lett. **70**,1385 (1993).
[16] Z. Ren, B. Chen, Z. Ma, and G. Xu, *Phys. Rev.* C **53**, R572(1996).
[17] B. A. Brown and P. G. Hansen, *Phys. Lett.* B **381**, 391 (1996).
[18] A. Navin, *et al*., *Phys. Rev. Lett*. **81**, 5089 (1998).
[19] H. Y. Zhang *et al*., *Nucl. Phys.* A **707**, 303 (2002).
[20] M. V. Zhukov and I. J. Thompson, *Phys. Rev.* C **52**, 3505 (1995).
[21] Z. Li, W. Liu, X. Bai, Y. Wang, G. Lian, Z. Li, and S. Zeng, *Phys. Lett.* B **527**, 50 (2002).
[22] T. Suda, K. Maruyama, and I. Tanihata, RIKEN Accel. Prog.Rep. **34**, 49 (2001).
[23] An international accelerator facility for beams of ions and antiprotons,GSI report (2002).
[24] A.Bhagwat, Y. K.Gambhira and S. H.Patil *Eur. Phys. J.* A **8**, 511 (2000).
[25] P. J.Brussard and P. W. M.Glademans, *Shell-model Application in Nuclear Spectroscopy* (North-Holland Publishing Company, Amsterdam) (1977).
[26] B. A. Brown, S. E. Massen and P. E. Hodgson, *Journal of Physics G* **5**, 1655 (1979).
[27] L. R. B. Elton and A. Swift, *Nucl. Phys*. A **94**, 52 (1967).
[28] S. Gamba, G. Ricco and G. Rottigni, *Nucl. Phys.* A **213**, 383 (1973).
[29] P. Ring and P.Schuck, *The Nuclear Many-Body Problem* (Springer-Verlag) (1981).
[30] L. G.Qiang, *J. Phys. G. Nuclear and Particle Physics***17**, 1(1991).
[31] T. Stovall, J. Goldemberg and D. B. Isabelle, *Nucl.Phys*. **86**,225 (1966).
[32] M. Wang *et al*. *Chin. Phys*. C **36**, 1603 (2012).
[33] G. Audi *et al*. *Chin. Phys*. C **36**, 1157 (2012).
[34] B. A. Brown and W. D. M. Rae, *Nuclear Data Sheets* **120**, 115 (2014).
[35] C. J. V. Der Poel *et al*., *Nucl. Phys.* A **373**, 81(1982).
[36] M. Fukuda *et al*., *Nucl. Phys.* A **656**, 209 (1999).
[37] A. Ozawa *et al*., *Phys. Lett.* B **334**, 18 (1994).
[38] K. Tanaka *et al*., *Eur. Phys. J.* A **25**, 221(2005).
[39] T. Stovall, J Goldemberg and D B Isabelle, *Nucl. Phys.* **86**, 225 (1966).
[40] C. Li, M. R. Yearian and I. Sick, *Phys. Rev*. C **9**, 1861 (1974).